

# Unique Interweaved Microtubule Scaffold Mediates Osmosensory Transduction via Physical Interaction with TRPV1

Masha Prager-Khoutorsky,<sup>1</sup> Arkady Khoutorsky,<sup>2</sup> and Charles W. Bourque<sup>1,\*</sup>

<sup>1</sup>Center for Research in Neuroscience, Research Institute of the McGill University Health Centre, Montreal General Hospital, Montreal, QC H3G 1A4, Canada

<sup>2</sup>Department of Biochemistry and Rosalind and Morris Goodman Cancer Research Centre, McGill University, Montreal, QC H3A 1A3, Canada

\*Correspondence: [charles.bourque@mcgill.ca](mailto:charles.bourque@mcgill.ca)

<http://dx.doi.org/10.1016/j.neuron.2014.07.023>

## SUMMARY

The electrical activity of mammalian osmosensory neurons (ONs) is increased by plasma hypertonicity to command thirst, antidiuretic hormone release, and increased sympathetic tone during dehydration. Osmosensory transduction is a mechanical process whereby decreases in cell volume cause the activation of transient receptor potential vanilloid type-1 (TRPV1) channels to induce depolarization and increase spiking activity in ONs. However, it is not known how cell shrinking is mechanically coupled to channel activation. Using superresolution imaging, we found that ONs are endowed with a uniquely interweaved scaffold of microtubules throughout their somata. Microtubules physically interact with the C terminus of TRPV1 at the cell surface and provide a pushing force that drives channels activation during shrinking. Moreover, we found that changes in the density of these interactions can bidirectionally modulate osmosensory gain. Microtubules are thus an essential component of the vital neuronal mechanotransduction apparatus that allows the brain to monitor and correct body hydration.

## INTRODUCTION

Systemic osmoregulation is a vital process whereby changes in plasma osmolality detected by osmosensory neurons (ONs) modulate ingestive behavior, sympathetic outflow, and renal function to stabilize the tonicity and volume of the extracellular fluid (Bourque, 2008). Failure to osmoregulate can lead to irreversible organ injury and neurological trauma because of damaging changes in cell volume caused by acute hyperosmolality or hypoosmolality (Bourque, 2008). ONs in the hypothalamic supraoptic nucleus (SON) are intrinsically osmosensitive (Mason, 1980; Oliet and Bourque, 1992, 1993a, 1993b) and transduce increases in extracellular fluid osmolality, such as those that occur during dehydration, into increases in action potential discharge frequency. This enhanced electrical activity

causes antidiuretic hormone (vasopressin) release into the bloodstream and thereby promotes water reabsorption at the kidney to restore hydromineral homeostasis (Bourque, 2008).

Osmosensory transduction in ONs is mediated by an N-terminal variant of transient receptor potential vanilloid type-1 (TRPV1), a nonselective cation channel that is activated during hypertonicity-evoked shrinking (Ciura and Bourque, 2006; Sharif Naeini et al., 2006). The membrane depolarization and increased action potential firing caused by decreases in the volume of ONs is equivalent whether shrinking is evoked by hypertonicity or by negative pressure applied through a patch pipette. Thus, osmosensory transduction does not rely on changes in the concentration of intracellular solutes or ionic strength but is a mechanical process mediated by the decrease in cell volume (Zhang et al., 2007; Ciura et al., 2011). The mechanisms by which decreases in cell volume are coupled to the activation of TRPV1 in ONs are unknown. However, previous studies have shown that microtubules can interact with TRPV1 *in vitro* (Goswami et al., 2004; Goswami et al., 2007) and that microtubule networks can undergo compression when physically constrained (Janson et al., 2003; Dogterom et al., 2005; Brangwynne et al., 2006). Therefore, we hypothesized that microtubules may play a direct role in osmosensory transduction by coupling changes in cell volume to channel activation.

## RESULTS

### Microtubule Organization in ONs

Previous work has shown that the magnitude of the cation current activated by hypertonicity in acutely isolated ONs is similar to that generated by intact ONs recorded *in situ*, suggesting that transduction occurs primarily in the soma of these cells (Bourque, 1989; Oliet and Bourque, 1993a, 1993b). We therefore compared the organization of microtubules in the somata and proximal dendrites of ONs and nonosmosensitive neurons using superresolution imaging with structured illumination microscopy (SIM). SIM analysis of immunostained tissue sections revealed an equivalent density of microtubules in the dendrites of ONs, cortical, and hippocampal neurons (Figures 1A–1G and Figure S1 available online). However, we found that microtubule density was significantly higher in the somata of ONs than in other types of neurons (Figures 1A–1C, 1I–1K, and 1O). Moreover, microtubules in the somata of ONs formed a highly

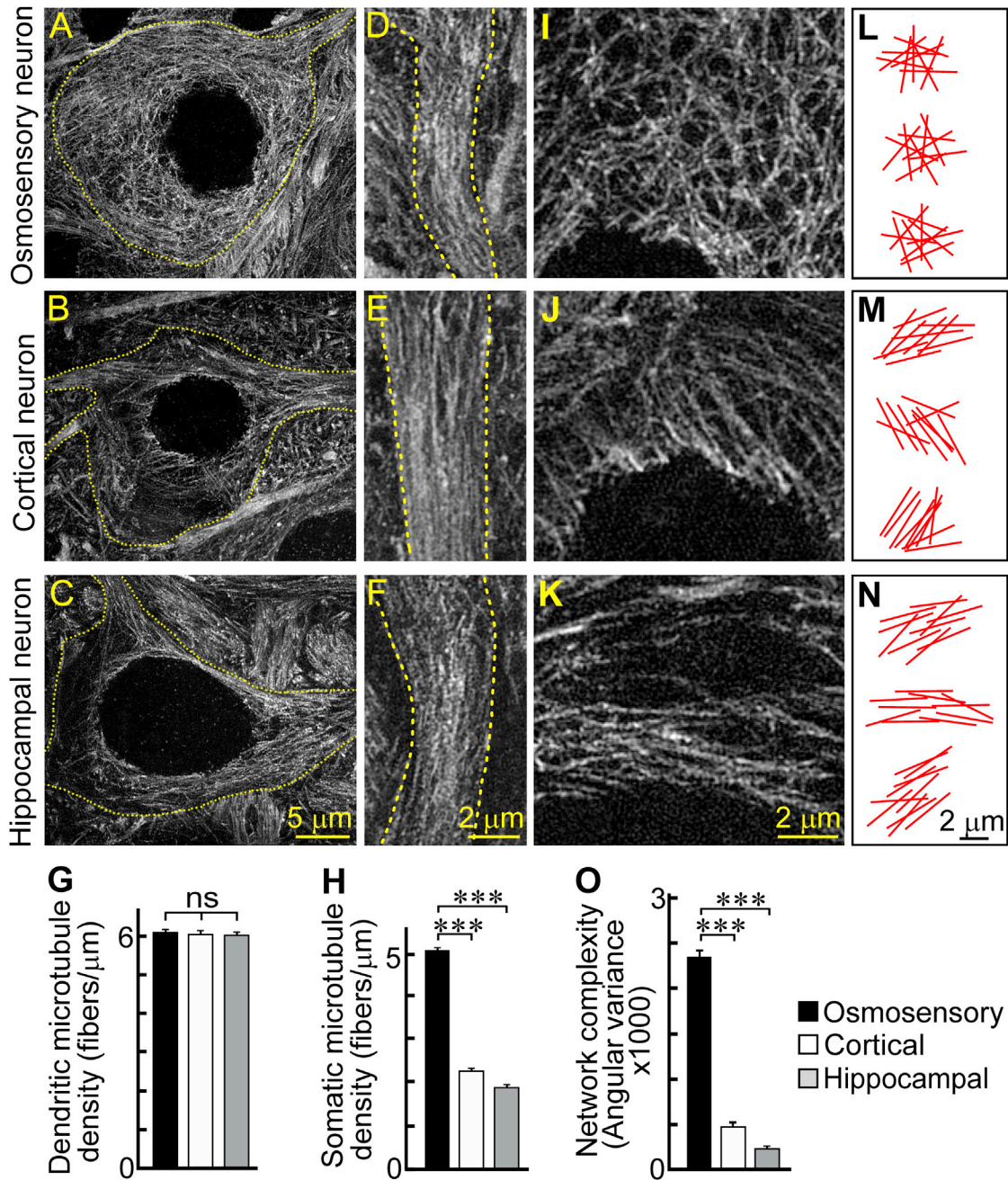


### Figure 1. ONs Feature a Prominent Somatic Microtubule Network

(A–C) Immunostaining for  $\alpha$ -tubulin in adult rat brain sections analyzed by superresolution structured illumination microscopy (SIM) reveals microtubule network organization in different types of neurons: osmosensory neuron (ON) (A), cortical neuron (B), and hippocampal neuron (C). Dotted lines (A–C) delineate cell perimeters (Figure S1).

(D–F) Higher-magnification images of proximal dendrites of ON (D), cortical (E), and hippocampal (F) neurons.

(G) Density of microtubules in dendrites of 20 ONs, cortical, and hippocampal neurons from four animals.

(H) Density of microtubules in somata of different types of neurons (Figure S1) ( $n = 82$  for ONs,  $n = 35$  for cortical, and  $n = 54$  for hippocampal neurons).

(I–K) Higher-magnification images of the somata of ON (I), cortical (J), and hippocampal (K) neurons.

(L–N) Stick diagrams show the position and orientation of 10 skeletonized microtubules detected within small regions of the cytoplasm for three different cells (data not shown) in each class of neuron: osmosensory (L), cortical (M), and hippocampal (N).

(O) Network complexity, quantified as angular variance, in the three subtypes of neurons ( $n = 20$  each). Data are presented as mean  $\pm$  SEM. \*\*\* $p < 0.001$ ; ns, not significant.

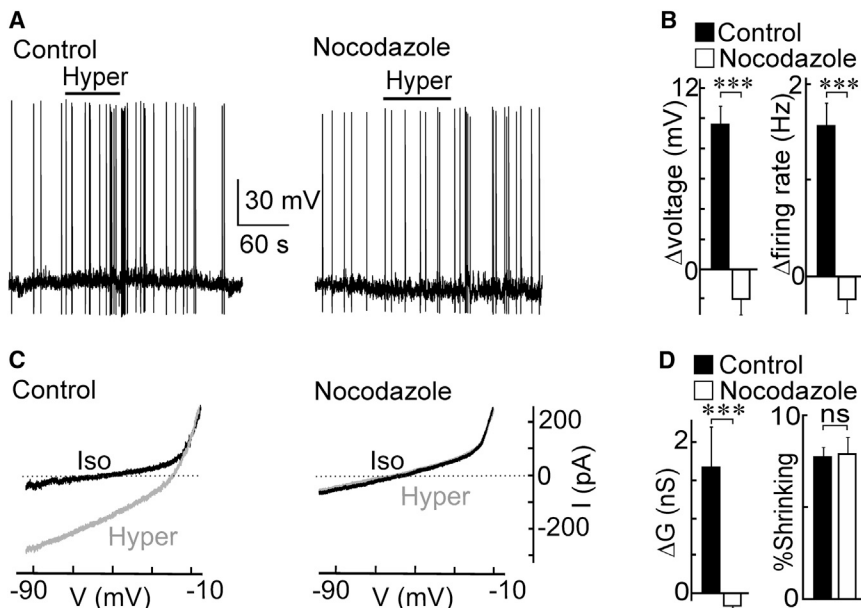


**Figure 2. Microtubules Are Required for Osmosensory Transduction**

(A) Whole-cell current-clamp recordings from ONs show the effects of hypertonicity (+25 mM mannitol, bars) on membrane voltage in control and nocodazole-treated ONs (0.5  $\mu$ M).

(B) Hypertonicity-induced changes ( $\Delta$ ) in membrane voltage and firing rate in control (n = 11) and nocodazole-treated ONs (n = 6).

(C) Traces show whole-cell current-voltage (I-V) relations measured under isotonic (black) and hypertonic conditions (+50 mM mannitol; gray) in representative control and nocodazole-treated ONs. Dotted lines indicate zero current.

(D) Hypertonicity-induced changes in membrane conductance ( $\Delta$ G) and cell volume (% Shrinking) in control (n = 8) and nocodazole-treated ONs (n = 12). Data are presented as mean  $\pm$  SEM. \*\*\*p < 0.001; ns, not significant.

interweaved 3D network that occupied the full volume of the perinuclear cytoplasm, as compared to the sparse and rectilinear arrays observed in other types of neurons (Figures 11–10) and commonly reported in other studies (Baas et al., 1987; Burton, 1992; Nixon, 1998).

### Microtubules Are Essential for Osmotic and Mechanical Transduction in ONs

To determine whether microtubules are required for osmosensory transduction, we first examined the effects of the microtubule-disrupting agent nocodazole (Samson et al., 1979; Jordan et al., 1992) on ONs acutely isolated from the SON of adult rats. As illustrated in Figure S2, the somata of untreated ONs preserved a highly interweaved microtubule scaffold similar to that of ONs in situ. Current-clamp recordings showed that increasing the osmolality of the perfusing solution by the addition of mannitol caused a depolarization of the membrane potential and an increase in action potential firing rate in control ONs, but these effects were abolished in cells that had been pretreated with 0.5  $\mu$ M nocodazole for 15–40 min (Figures 2A and 2B). Similarly, nocodazole treatment eliminated the hypertonicity-induced increases in membrane conductance observed in control cells (Figures 2C and 2D), despite an equivalent degree of shrinking in both groups of ONs (Figure 2D).

Since the effects of hypertonicity on ONs are caused by a mechanical activation of the transduction channels (Oliet and Bourque, 1993b; Zhang et al., 2007), we hypothesized that disrupting microtubules should also interfere with responses to shrinking induced by application of negative pressure to the recording pipette. Indeed, mechanically evoked shrinking caused a depolarization and excitation of control cells, but not nocodazole-treated ONs (Figures 3A and 3B). Similarly, increases in membrane conductance induced by the application of negative pressure in control ONs were absent in nocodazole-treated cells (Figures 3C and 3D), despite equivalent de-

creases in ON volume (Figure 3D). By contrast, ONs pretreated with the microtubule-stabilizing compound taxol (5  $\mu$ M; 15–40 min) (Downing, 2000) displayed enhanced responses under both current-clamp (Figures 3A and 3B) and voltage-clamp conditions (Figures 3C and 3D).

### Microtubules Interact with TRPV1 in ONs

The ion channel responsible for osmosensory transduction in ONs is an N-terminal variant of TRPV1 that bears an intact cytoplasmic C terminus (Sharif Naeini et al., 2006). Previous in vitro studies have shown that TRPV1 can directly interact with microtubules through a pair of binding sites for  $\beta$ -tubulin located in the channel's C terminus (Goswami et al., 2004, 2007). We therefore hypothesized that a tubulin-TRPV1 interaction is required for the mechanical excitation of ONs during cell shrinking. To determine whether tubulin interacts with TRPV1 in vivo, we immunoprecipitated extracts prepared from rat SONs with anti-TRPV1 antibody. Tubulin coimmunoprecipitated with TRPV1, revealing the presence of a physical interaction between these proteins in SON (Figure 4A). To determine whether tubulin and TRPV1 interact in intact ONs, we next performed a proximity ligation assay (PLA) that allows detection of proteins that are colocalized at the nanoscale in situ. The PLA approach involves fluorescence detection of a polymerase chain reaction (PCR) amplicon whose production is conditional on the colocalization of oligonucleotides brought together by antibodies targeting the selected pair of antigens (see Experimental Procedures) (Söderberg et al., 2006; Trifilieff et al., 2011). Application of the PLA approach in acutely isolated ONs revealed multiple sites of tubulin-TRPV1 interaction (Figures 4B–4D). Notably, the majority of tubulin-TRPV1 interactions were observed on the surface of ONs, where transduction is presumed to occur (Figure 4E).

### Effects of Nocodazole and Taxol on Tubulin-TRPV1 Interactions

The findings above indicate that microtubules might extend all the way to the plasma membrane where they interact with

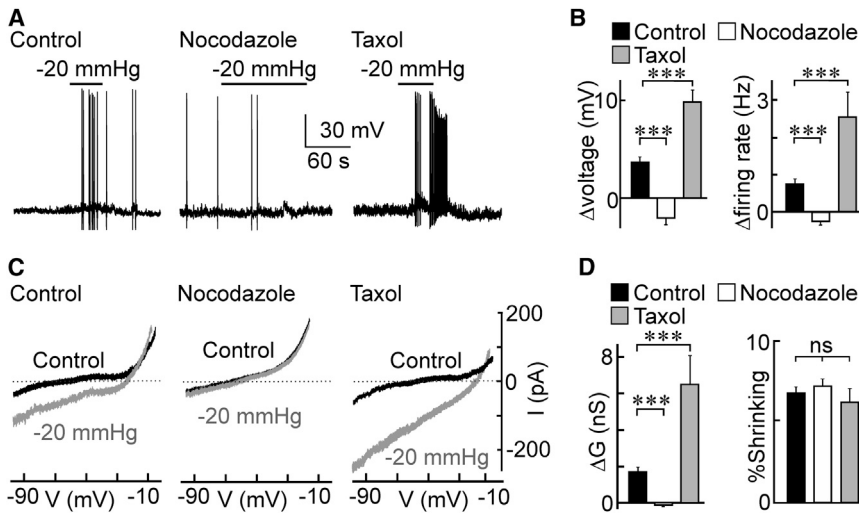


**Figure 3. Microtubules Are Required for Mechanotransduction**

(A) Representative voltage traces showing effects of negative pressure applied to the patch pipette ( $-20$  mmHg, bars) on control (left), nocodazole- (middle), and taxol-treated ONs (right). (B) Suction-induced changes ( $\Delta$ ) in membrane voltage and firing rate in control ( $n = 28$ ), nocodazole- ( $n = 16$ ), and taxol-treated ONs ( $n = 9$ ). (C) I-V relations measured under voltage clamp before (control, black) and after applying suction ( $-20$  mmHg, gray) in control, nocodazole-, and taxol-treated ONs. Dotted lines indicate zero current. (D) Suction-induced changes in membrane conductance ( $\Delta G$ ) and cell volume (% Shrinking) in control ( $n = 24$ ), nocodazole- ( $n = 18$ ), and taxol-treated cells ( $n = 6$ ). Data are presented as mean  $\pm$  SEM. \*\*\* $p < 0.001$ ; ns, not significant.

TRPV1 channels on the cell surface. Therefore the effects of nocodazole and taxol on mechanical transduction could be mediated either through a modulation of the density of these interaction sites or through an effect on the integrity of the microtubule scaffold. SIM analysis revealed that nocodazole has no effect on the density or complexity of the somatic microtubule network (Figures 5A, 5B, 5D, and 5E). Similarly, taxol only caused a slight increase ( $\sim 25\%$ ) in somatic microtubule density and had no effect on network complexity (Figures 5C–5E).

We therefore specifically examined the nature of the submembrane microtubule network using SIM on cells in which tubulin was labeled using immunohistochemistry and the plasma membrane was labeled with Dil. As illustrated in Figure 5F, microtubules were commonly observed to approach and contact the plasma membrane. Moreover, inspection of cell regions displaying intense staining of both microtubules and plasma membrane showed that treatment of ONs with taxol or nocodazole does not affect the integrity of the submembrane microtubule network or the density of sites at which microtubules appear to reach the plasma membrane (Figures 5G–5I) (see [Experimental Procedures](#)).

In agreement with these observations, previous studies have shown that low concentrations of nocodazole do not affect the integrity of microtubules but can displace proteins that bind at the plus end of microtubules (Stepanova et al., 2003; Jaworski et al., 2009; Baas and Ahmad, 2013). To test the hypothesis that low doses of nocodazole release TRPV1 from the microtubule tips at the cell surface by disrupting the tubulin-TRPV1 interaction, we examined the effects of  $0.5 \mu\text{M}$  nocodazole on interaction sites detected using the PLA approach. Indeed, nocodazole dramatically decreased the number of sites at which tubulin and TRPV1 interact on the surface of ONs (Figures 5J, 5K, and 5M). Conversely, the density of tubulin-TRPV1 interaction sites was almost doubled on the surface of ONs treated with  $5 \mu\text{M}$  taxol (Figures 5L and 5M). These results suggest that effects of nocodazole and taxol on osmosensory transduction are mediated by their ability to modulate the density of tubulin-TRPV1 interaction sites rather than by affecting the organization of the microtubule network.

### Disruption of Tubulin-TRPV1 Interaction Blocks Mechanotransduction

Previous work has shown that TRPV1 can interact with microtubules via a pair of tubulin-binding domains located in the channel's cytoplasmic C terminus (Figure S3) (Goswami et al., 2004, 2007). To examine whether these interaction sites are involved in mediating mechanotransduction, we examined the effects of specifically disrupting tubulin-TRPV1 interaction at these sites on responses induced by shrinking in ONs. To perform this experiment, we generated three synthetic peptides (P1, P2, P3), whose sequences corresponded to the two tubulin-binding domains (P1 and P2, respectively), and to a nonoverlapping portion of the C terminus to be used as a control (P3; Figure S3) (Goswami et al., 2007). As illustrated in Figure 6A, addition of P1, P2, or P1+P2 significantly interfered with the coimmunoprecipitation of tubulin and TRPV1 in SON lysates, whereas P3 had no effect (Figures 6A and 6B). Thus, P1 and P2 can be used to disrupt the tubulin-TRPV1 interaction, while the P3 peptide can be used as a control.

To examine the effect of perturbing the tubulin-TRPV1 interaction on mechanotransduction in isolated ONs, we included synthetic peptides in the solution filling the recording pipettes and recorded mechanically evoked responses at least 20 min after establishing the whole-cell configuration (Figure S4A). While negative pressure caused a similar degree of shrinking in all groups (Figure S4B), excitation was observed only in cells loaded with P3 or vehicle, but not when P1 or P2 were dialyzed into the cells (Figures 6C and 6D). Similarly, suction-induced increases in membrane conductance were abolished by inclusion P1 or P2 peptides in the recording pipette (Figures 6E and 6F).

To determine whether TRPV1 channels disconnected from microtubules can be still activated by other (nonmechanical) stimuli, we examined the effect of bath-applying angiotensin II, a neuropeptide that exclusively activates TRPV1 in ONs of the SON via G protein-coupled PKC/PLC pathway (Chakfe and Bourque, 2000; Sharif Naeini et al., 2006). Application of angiotensin II was found to activate TRPV1 in ONs that had been rendered insensitive to mechanical stimulation by loading with P1 and P2 peptides (Figures 6G and 6H; Figure S5). Thus,

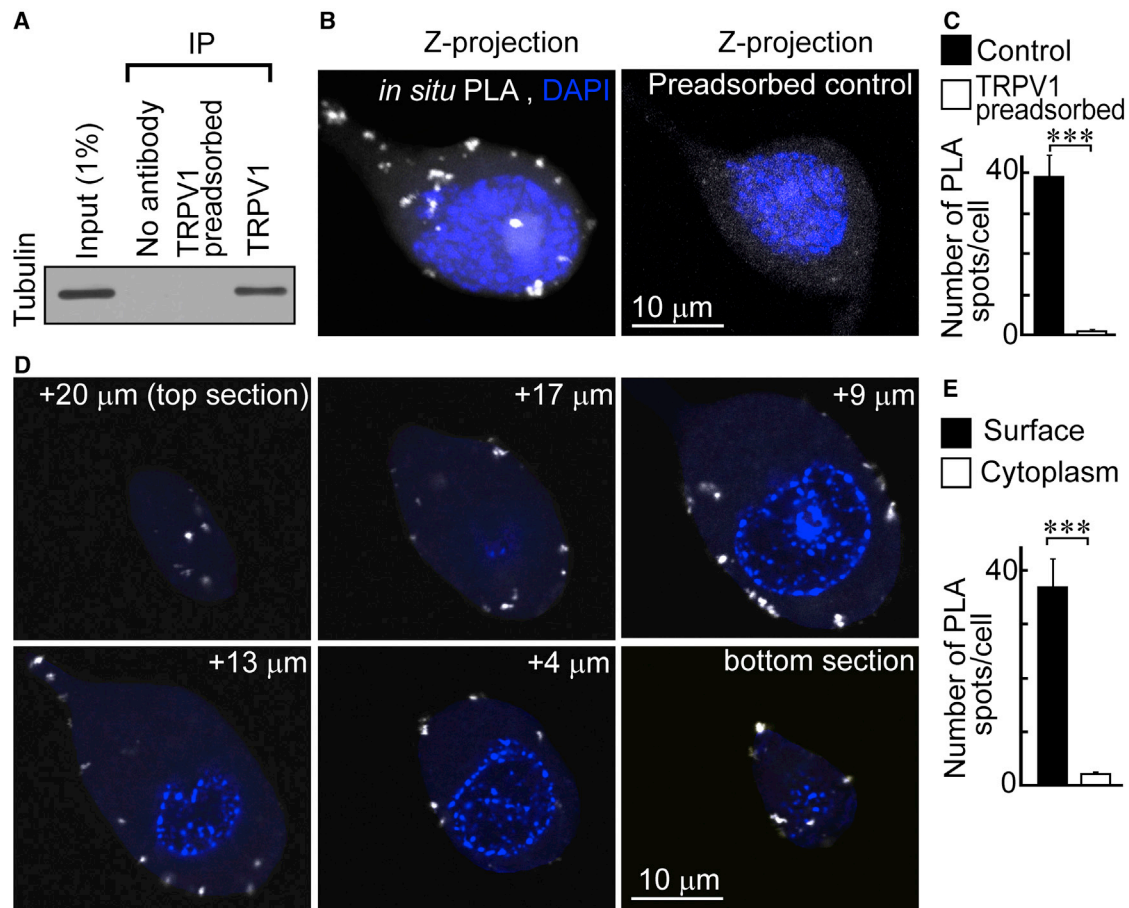


**Figure 4. Microtubules Interact with TRPV1**

(A) SON lysates were immunoprecipitated with TRPV1 antibody and western blotted for tubulin. A 55 kDa band corresponding to tubulin was detected ( $n = 3$ ). No tubulin was detected without TRPV1 antibodies (No antibody) or when TRPV1 antibodies were preadsorbed with the antibody inhibitory peptide (TRPV1 preadsorbed).

(B) In situ proximity ligation assay (PLA) to visualize proximate protein interactions by combining antibody-antigen binding with PCR and followed by the fluorescent labeling of the PCR product (in situ PLA signal). The images show maximum intensity projection of in situ PLA signal using TRPV1 and tubulin antibodies in isolated ONs. White spots represent sites where TRPV1 and tubulin colocalize at the nanoscale level, blue is DAPI. No interaction was detected when the TRPV1 antibody was preadsorbed.

(C) Total number of interaction sites in control cells ( $n = 25$ ) and cells where TRPV1 was preadsorbed ( $n = 6$ ).

(D) PLA signal and DAPI at different confocal planes (indicated at the top of each panel) in a single representative ON.

(E) Mean number of PLA spots detected on the surface (within  $1 \mu\text{m}$  from the cell perimeter) and in the cytoplasm of 25 ONs (from 4 animals). Data are presented as mean  $\pm$  SEM. \*\*\* $p < 0.001$ .

displacement of the tubulin-TRPV1 interaction can specifically abolish mechanical regulation of TRPV1 channels, without preventing the activation of these channels by other forms of signaling.

#### Working Model for Mechanical Gating of TRPV1

Taken together, the findings described above suggest that two models should be considered to explain the mechanical gating of TRPV1 by microtubules in ONs. In the first model (the *association model*; Figure 7A), the inward movement of the plasma membrane caused by cell shrinking would promote an increase in the number of TRPV1 channels that interact with microtubules, and channel activation would result directly from the establishment of this interaction. In the second model (the *push-activation*

*model*; Figure 7B), only TRPV1 channels with a preexisting interaction with microtubules would be available for activation. In this case, the inward movement of the plasma membrane would presumably compress the microtubules and generate a push force that leads channel activation. To resolve between these possibilities, we examined the effect of hypertonicity-induced shrinking on the density of TRPV1-tubulin interaction sites detected by the PLA method. Despite the pronounced increase in membrane conductance provoked by hypertonicity (Figures 2C and 2D), this stimulus failed to increase the number of interaction sites observed on the surface of ONs (Figures 7C and 7D).

If TRPV1 activation is mediated by application of a push force via an attached microtubule, then this process should occur with little delay (Christensen and Corey, 2007). To determine whether

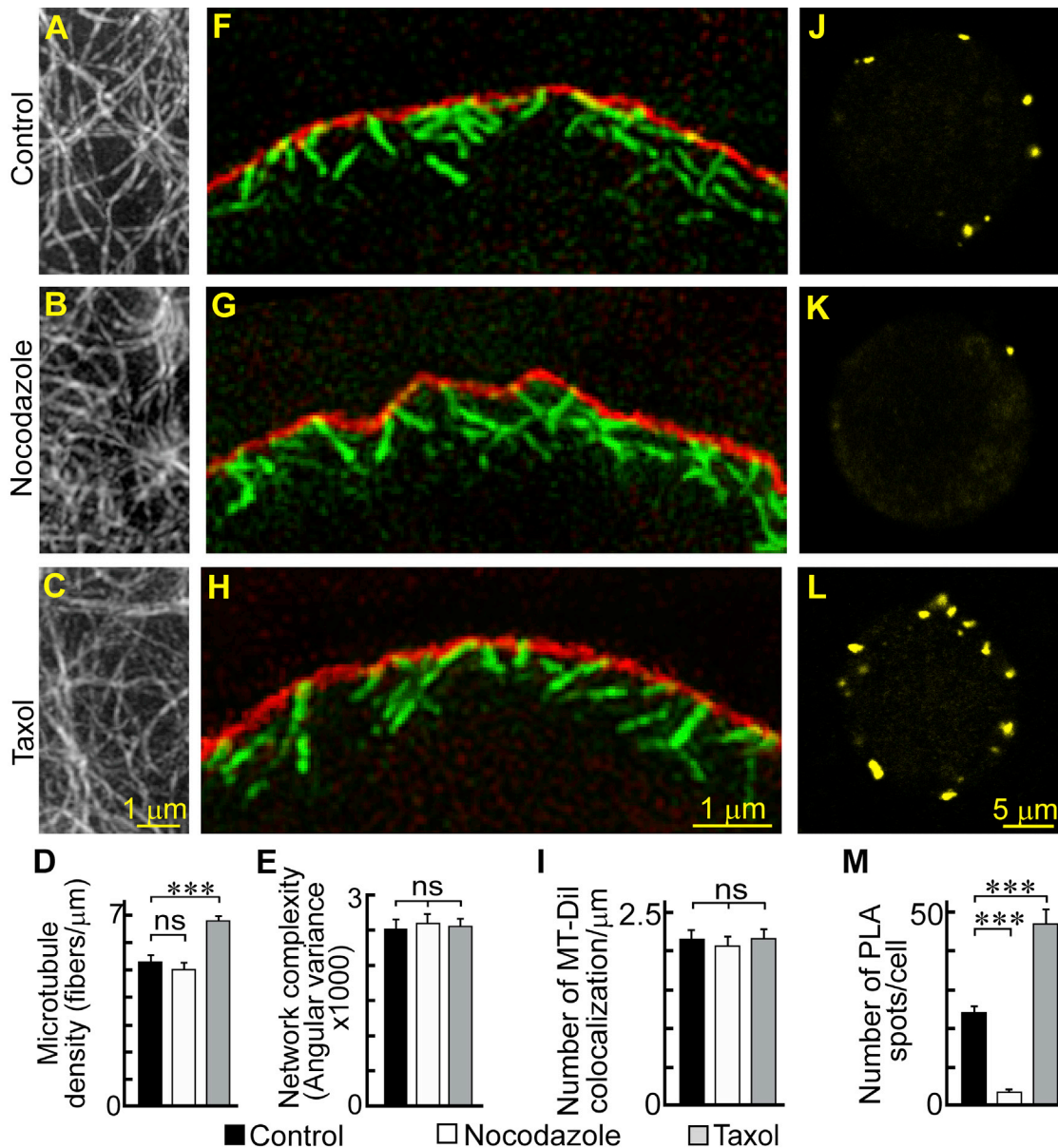


**Figure 5. Effect of Nocodazole and Taxol on Microtubule Organization and Tubulin-TRPV1 Interaction Sites**

(A–C) Immunostaining of  $\alpha$ -tubulin in acutely isolated ONs observed by SIM shows the somatic microtubule network in control (A), 0.5  $\mu$ M nocodazole- (B), and 5  $\mu$ M taxol-treated cells (C).

(D) Mean somatic microtubule density in control (n = 10), nocodazole- (n = 10), and taxol-treated ONs (n = 10).

(E) Mean angular variance as a measure of network complexity in the same groups of cells.

(F–H) SIM images of  $\alpha$ -tubulin (green) and plasma membrane (red) illustrate submembrane microtubule organization in control (F), nocodazole- (G), and taxol-treated ONs (H).

(I) Mean density of sites at which microtubules contact the plasma membrane in groups of control (n = 12), nocodazole- (n = 13), and taxol-treated ONs (n = 12).

(J–L) PLA signal observed across the middle confocal section of representative control (J), nocodazole- (K), and taxol-treated ONs (L).

(M) Mean number of PLA spots detected on the surface control (n = 36), nocodazole-treated (n = 36), and taxol-treated (n = 50) ONs (from 6 animals). Data are presented as mean  $\pm$  SEM. \*\*\*p < 0.001; ns, not significant.

transduction channels can be activated with rapid kinetics, we performed cell-attached recordings from ONs and examined the effects of suddenly displacing the membrane in an inward direction using a high-speed pressure clamp (Figure 8A; see

Experimental Procedures). As illustrated in Figures 8B and 8C, small increases in pipette pressure caused a rapid and reversible activation of cation channels with a unitary amplitude of  $\sim 2$  pA. Although the probability of channel opening increased gradually

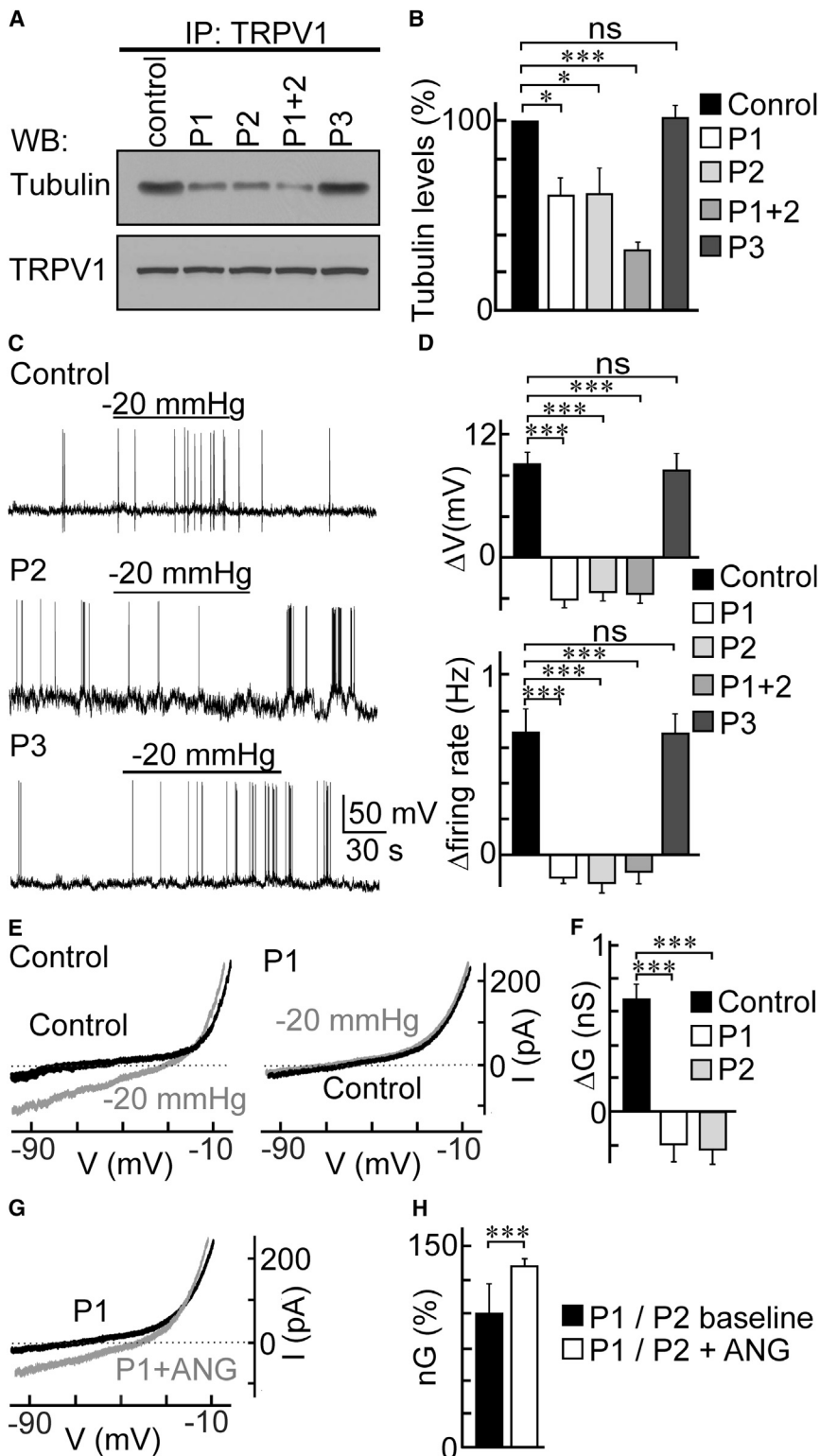


**Figure 6. Tubulin-TRPV1 Interaction Is Required for Mechanotransduction**

(A) SON lysates were immunoprecipitated with TRPV1 antibody and the denatured product was western blotted for tubulin and TRPV1. Although an equivalent amount of TRPV1 was precipitated in each condition (bottom), the tubulin signal was reduced when lysates (top) were pretreated with P1, P2, and P1+P2 but not P3 synthetic peptides (Figure S3).

(B) Normalized intensity of the tubulin bands detected in all conditions ( $n = 3$ ).

(C) Representative voltage traces show the effects of mechanical stimulation (bars) on cells recorded with pipettes containing vehicle (control, DMSO), P2, or P3 (Figure S4).

(D) Suction-induced changes in membrane voltage (top) and firing rate (bottom), (control,  $n = 15$ ; P1,  $n = 8$ ; P2,  $n = 9$ ; P1+P2,  $n = 9$ ; P3,  $n = 10$ ).

(E) I-V relations in control conditions (black) and after suction (-20 mmHg, gray) in control (left, DMSO) and P1-loaded cell (right).

(F) Suction-induced changes in membrane conductance ( $\Delta G$ ) in vehicle-treated ONs (control,  $n = 10$ ) and cells loaded with P1 ( $n = 7$ ) or P2 ( $n = 9$ ).

(G) I-V relations in P1-loaded ON before (black) and after bath application of 1  $\mu$ M angiotensin II (P1+ANG, gray). Dotted lines indicate zero current.

(H) Normalized conductance of ONs loaded with P1 or P2 before (P1/P2 baseline) and after application of angiotensin II (P1/P2+ANG;  $n = 10$ ), (Figure S5). Data are presented as mean  $\pm$  SEM. \* $p < 0.05$ ; \*\*\* $p < 0.001$ ; ns, not significant.

push-activation model as the basis for osmosensory transduction.

## DISCUSSION

Many types of mechanosensitive cells feature unique molecular architectures that allow them to detect forces associated with physical sensory stimuli (e.g., touch and hearing) and visceral interoceptive signals such as arterial blood pressure and fluid osmolality (Chalfie, 2009; Marshall and Lumpkin, 2012). A common requirement in these cells is that stimulus-dependent forces dynamically modulate the activity of a mechanosensitive ion channel to generate receptor potentials that change neuronal firing in a manner that faithfully encodes the original stimulus. Previous work has shown that cytoskeletal proteins including actin, cadherins, and myosins can contribute to many forms of mechanotransduction

following the onset of the pressure pulse (Figure 8D), the latency to first opening was quite rapid (range 4–196 ms, median 54 ms;  $n = 60$ ; Figure 8E). Collectively, these observations support a

(Christensen and Corey, 2007; Zhang et al., 2007; Sharif-Naeini et al., 2009; Hoffman et al., 2011; Tyler, 2012). In most cases, these proteins are localized to specialized subcellular regions

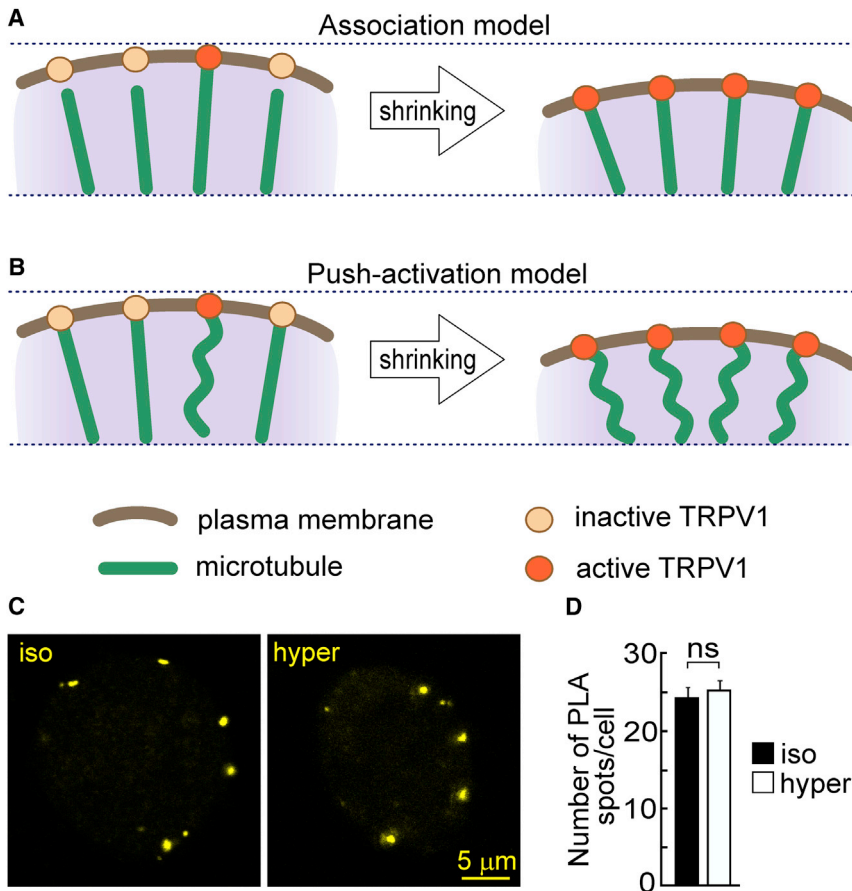


**Figure 7. Models of Shrinking-Mediated Activation of TRPV1 in ONs**

(A) The association model: at rest (left) most of the cell surface transduction channels are inactive because they are not in contact with microtubules. Cell shrinking narrows the gap between microtubules and the plasma membrane (right), thereby increasing the fraction of TRPV1 channels that become activated as a result of binding to microtubules.

(B) The push-activation model: at rest many TRPV1 channels are bound to microtubules, but few are activated due to the lack of sufficient pushing force (left). As a result of cell shrinking, the plasma membrane shifts inward (right), increasing the proportion of microtubules that push onto (and activate) TRPV1 channels.

(C) PLA signal observed across the middle confocal section of isolated ONs exposed to isotonic (iso) or hypertonic solution (hyper; +25 mM mannitol).

(D) Mean number of PLA spots detected on the surface of ONs in isotonic ( $n = 36$  from 6 animals) and hypertonic conditions (white,  $n = 39$  from 6 animals). Data are presented as mean  $\pm$  SEM. ns, not significant.

(e.g., cilia) or extracellular structures (e.g., tip-links in vertebrate hair cells), where they may play an active role in the transduction process (Chalfie, 2009). Surprisingly, little is known concerning the possible role of microtubules in mechanotransduction.

Although microtubules are best known for their important roles in intracellular transport and cell division, they are also recognized as the cytoskeleton's strongest filaments (Dogterom et al., 2005; Fletcher and Mullins, 2010) and thus play determinant roles in the control of cell morphology and in the generation of directed forces that drive changes in cell shape (Ingber, 2003; Fletcher and Mullins, 2010). Early studies exploring touch-insensitive mutants of *C. elegans* suggested that microtubules might play an important role in mechanotransduction at the whole organism level (Chalfie and Sulston, 1981; Chalfie and Au, 1989). However, more recent studies have shown that genetic elimination of touch neuron-specific microtubules does not fully abolish mechanosensitive currents (O'Hagan et al., 2005) and that enzymatic disruption of microtubule organization does not impair touch sensitivity (Topalidou et al., 2012). The involvement of microtubules as mediators of mechanotransduction in *C. elegans* therefore remains unclear.

Recent studies have shown that the no mechanoreceptor potential C (*nompC*) gene encodes a mechanically gated ion channel involved in gentle touch sensation in *Drosophila* (Cheng et al., 2010; Yan et al., 2013) and that ankyrin domains within the NOMPC protein form an intracellular filament that tethers these

we show that microtubules play an essential role in the mechanical activation of transduction channels in ONs of the rat hypothalamus.

#### ONs Feature a Unique Interweaved Microtubule Scaffold

Using superresolution imaging with SIM, we found that the soma of ONs comprises a remarkably dense microtubule scaffold that fully occupies the cytoplasm of these cells, from the nucleus to the plasma membrane. These microtubules are positioned in a wide variety of angles relative to each other, thereby creating a highly interweaved network. This previously undescribed architecture contrasts sharply with the rectilinear organization of microtubules commonly observed with other imaging methods in the axons and dendrites of other types of neurons (e.g., Stuess and Bradke, 2011), and with the centrosome-oriented microtubules typically found in nonneuronal cells (Luxton and Gundersen, 2011; Vignaud et al., 2012).

The uniqueness of the interweaved scaffold we observed in ONs was confirmed by SIM analysis in other parts of the brain. Indeed, the density and angular variance of cytoplasmic microtubules were found to be significantly lower in cortical and hippocampal neurons (CA3 and dentate gyrus) than in ONs in the SON (Figure 1). Similarly, the complexity and density of the cytoplasmic microtubule network observed in neurons of the cerebellum (Purkinje and granule cells) and suprachiasmatic nucleus were much less than that observed in the SON (data not shown).

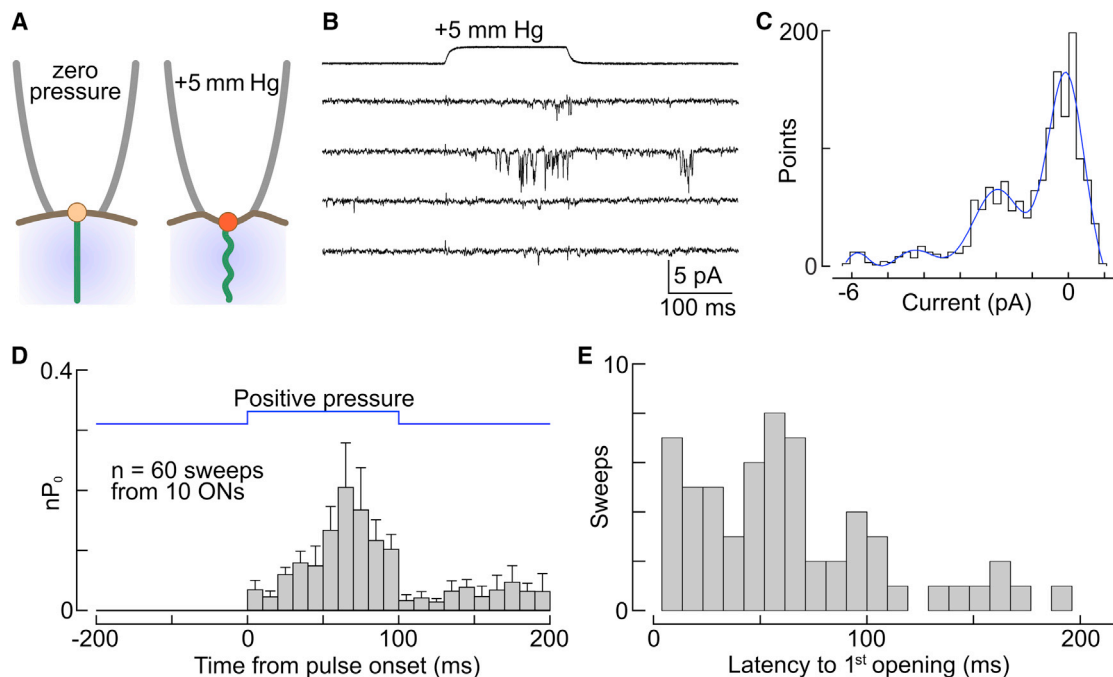


**Figure 8. Kinetics of Channel Activation during Mechanical Stimuli**

(A) Schematic illustrating the application of the pressure-clamp technique in cell-attached mode.

(B) Four sweeps obtained by cell-attached current recording ( $V_{\text{pipette}} +40$  mV) illustrate the effect of a pressure step (top trace) on channel activity recorded from an isolated ON. At least three channels are present in this example.

(C) All-points histogram plotting the amplitudes of current samples recorded during the active portion of the second sweep in (B).

(D) Changes in mean ( $\pm$ SEM) probability of opening ( $nP_0$ ) observed during 60 pressure pulses recorded from ten ONs (see [Experimental Procedures](#)).

(E) Bar histogram plots the distribution of latencies to first opening after the onset of the 60 pressure steps analyzed in (D).

Remarkably, we observed densely interweaved microtubule networks in the cytoplasm of ONs present in other parts of the hypothalamus, including those in the organum vasculosum laminae terminalis and in the magnocellular division of the paraventricular nucleus (data not shown). Therefore, ON somata display a uniquely dense and interweaved scaffold of microtubules that may be important for osmosensory transduction.

#### Tubulin-TRPV1 Interaction Is Necessary for Mechanotransduction

Using superresolution imaging with SIM, we found that microtubules extend all the way to the surface of ONs, where they appear to establish close contacts with the plasma membrane. Moreover, a combination of biochemical experiments and nanoscale imaging revealed that tubulin interacts with TRPV1 on the cell surface, and electrophysiological recordings showed that shrinking-induced excitation of ONs is blocked when this interaction is prevented by peptides that specifically interfere with the binding of tubulin to TRPV1.

We also found that pretreatment of ONs with nocodazole inhibits the excitatory response induced by mechanical or osmotically induced shrinking. Notably, this blocking effect of nocodazole was accompanied by a pronounced reduction in the density of sites at which TRPV1 and tubulin interact on the surface of the ONs but not by a disruption of the integrity of the cytoplasmic or submembrane microtubule network.

Conversely, pretreatment with taxol increased the density of tubulin-TRPV1 interaction sites at the cell surface and potently enhanced the responses of ONs ( $\sim 300\%$ ) to shrinking. These observations indicate that an interaction between TRPV1 and tubulin is necessary for mechanotransduction to occur.

#### Push Activation of TRPV1 by Microtubules

Based on the observations summarized above, two distinct models could be used to explain the mechanical activation of TRPV1 during shrinking in ONs: an association model, in which TRPV1 channels are activated upon binding to tubulin, and a push-activation model, in which channels prelinked to microtubules are activated in response to compression force transmitted through the attached filament (Figures 7A and 7B). According to the first model, cell shrinking would cause an increase in the number of sites at which TRPV1 channels and microtubules physically interact due to an increase in their mutual proximity, thereby activating the channel as a result of the binding event. However, we found that the density of sites at which tubulin and TRPV1 interact does not increase when ONs undergo shrinking caused by a hypertonic stimulus. An alternative possibility consistent with the association model is that this increased proximity induces a transduction current through a tubulin-mediated assembly of functional TRPV1 tetramers (Storti et al., 2012). However, whereas disruption of tubulin-TRPV1 interactions with synthetic peptides inhibited

the mechanical activation of TRPV1, it did not prevent the activation of these channels by a nonmechanical stimulus (e.g., angiotensin II), indicating that functional TRPV1 channels are constitutively expressed on the surface of ONs. Therefore, the activation of TRPV1 channels during acute mechanical or hypertonicity-evoked shrinking is unlikely to be mediated by the association model.

Although additional work is required to define the molecular basis for push activation of TRPV1 during shrinking in ONs, several possibilities can be considered (Christensen and Corey, 2007). First, push-activation of TRPV1 channels could be mediated indirectly, through an intermediate step. For example, a push force applied to the channel might cause a conformational change that enables its activation by another mediator, such as an enzyme or a second messenger. However, the involvement of an intermediate step seems unlikely, since channel activation occurred rapidly, often within a few milliseconds after pushing on the membrane (Figure 8). Push-activation of TRPV1 is therefore more likely to be mediated directly by the application of a compression force through the microtubule. Whether channel activation requires the application of force to the C terminus and/or forces applied at the channel-lipid interface as the complex is pushed outwardly by the microtubule remains to be determined.

Lastly, our data indicate that the sensitivity of osmosensory transduction can be modulated by changes in the density of sites at which tubulin and TRPV1 interact on the cell surface. Specifically, we found that the decreases and increases in interaction site density observed in ONs treated with nocodazole and taxol, respectively, were associated with proportional changes in the degree of shrinking-induced excitation (Figures 2 and 3) and basal membrane conductance (Figure S6).

### Significance of the Densely Interweaved Microtubule Scaffold

Previous studies have shown that interweaved networks of elastic filaments can distribute forces applied to one side of the cell toward the opposite side via tensigrity (Ingber, 2003). The dense and extensively interweaved network of microtubules observed in ONs may therefore serve to equilibrate changes in compression forces along the entire surface as cells undergo volume changes during osmotic perturbations. This feature could be important to maximize the number of channels that simultaneously monitor changes in the compression state of the microtubule scaffold as cells become exposed to a hyperosmotic environment. The dense microtubule scaffold could also serve to protect the structural integrity of ONs, as these cells do not regulate their volume when exposed to an osmotic stimulus (Zhang and Bourque, 2003).

### Concluding Remarks

A recent structural study has confirmed that at least one of the C-terminal tubulin-binding domains of TRPV1 is accessible for the binding of  $\beta$ -tubulin (Cao et al., 2013), and these domains are highly conserved across animal species, suggesting important roles in the regulation of this ion channel (Goswami and Hucho, 2008). Our study reveals that an interaction between tubulin and this domain is necessary to mediate the mechanical

activation of rat ONs during osmotically induced shrinking. Previous work has shown that the transduction channel in ONs is an N-terminal variant of TRPV1. Therefore, additional studies are required to determine whether microtubules can also mediate the mechanical regulation of the wild-type TRPV1 channel in nonosmosensitive cells, and if this form of regulation mediates any form of mechanosensation. Our findings reveal that microtubules play an essential role in the mechanical gating of transduction channels in ONs and expand our understanding of the mechanism by which the brain monitors and corrects the body's hydration state.

### EXPERIMENTAL PROCEDURES

#### Preparation of Isolated Cells

Male Long Evans rats (80–150 g; Charles River Laboratories) were used throughout this study and treated in strict accordance with the guidelines outlined by the Canadian Council on Animal Care (<http://www.ccac.ca/>) and experiments adhered to protocols approved by the Facility Animal Care Committee of McGill University. Briefly, rats were anesthetized with halothane (Sigma), were sacrificed by decapitation, and the brain was rapidly removed from the cranium and placed in chilled PIPES solution (pH 7.3) containing 120 mM NaCl, 5 mM KCl, 1 mM MgCl<sub>2</sub>, 10 mM PIPES, 1 mM CaCl<sub>2</sub>, and 10 mM glucose (osmolality adjusted to 295 mosmol/kg using mannitol). Blocks of tissue containing the supraoptic nuclei (~1 mm<sup>3</sup>) were removed using iridectomy scissors and placed in PIPES solution containing 0.7 mg/ml protease XIV (Sigma-Aldrich Canada) for 30 min. Tissue blocks were then transferred to protease-free PIPES solution, triturated using fire-polished Pasteur pipettes, and plated on plastic petri dishes or glass coverslips (for imaging experiments).

#### Cell Perfusion and Drug Application

For live cell recording or imaging (<2 hr after plating), dishes were placed on the stage of an IX-71 inverted phase-contrast microscope (Olympus Canada) and perfused with a HEPES-buffered saline solution (pH 7.3) containing 140 mM NaCl, 3 mM KCl, 1 mM MgCl<sub>2</sub>, 10 mM HEPES, 1 mM CaCl<sub>2</sub>, and 10 mM glucose; adjusted to 295 mosmol/kg with mannitol. Perfusion at 1.0–1.3 ml/min was achieved via a three barrel assembly controlled by an SF-77B fast-step device (Warner Instruments) that allows rapid switching between solutions. Ruthenium red (Sigma, 5  $\mu$ M) was dissolved in HEPES solution before every experiment. Nocodazole (Sigma-Aldrich Canada, 20 mM in DMSO) was dissolved into HEPES solution to a final concentration of 0.5  $\mu$ M. Taxol (Sigma-Aldrich Canada, 20 mM in DMSO) was dissolved into HEPES solution to a final concentration of 5  $\mu$ M. ONs were incubated for 15–40 min with nocodazole and taxol prior to delivering osmotic or mechanical stimuli. Hypertonic stimuli were applied via HEPES solution containing excess mannitol (+25 mM for current-clamp experiments and +50 mM for voltage-clamp experiments). Angiotensin II (Phoenix Pharmaceuticals) was diluted in HEPES to final concentration of 1  $\mu$ M immediately before application.

#### Measurement of Changes in Cell Volume

The degree of cell shrinking (expressed as percent change relative to control) was calculated from changes in maximal cross-sectional area (CSA) observed in control (CSA<sub>0</sub>) and test conditions (CSA) using the equation; % shrinking =  $100 \times [(CSA_0)^{1.5} - (CSA)^{1.5}] / (CSA_0)^{1.5}$  as previously described (Zhang and Bourque, 2003).

#### Electrophysiology

Membrane voltage or current was recorded using the whole-cell configuration of the patch-clamp technique as previously described (Oliet and Bourque, 1993b; Zhang et al., 2007). Briefly, cells were patch-clamped with glass pipettes containing a solution (pH 7.2) comprising 120 mM K-Gluconate, 1 mM MgCl<sub>2</sub>, 10 mM EGTA, 10 mM HEPES, and 4 mM Na<sub>2</sub>ATP, adjusted to 270 mosmol/kg. Tetrodotoxin (0.5  $\mu$ M; Alomone Labs) was added to the recording solution for voltage-clamp experiments. Recordings were done in the whole-cell mode using an Axopatch-200B amplifier (Molecular Devices).

Membrane current (d.c. - 2 KHz) was digitized at 10 kHz via a Digidata 1322A interface coupled to a PC running Clampex 8 (Molecular Devices). Whole-cell capacitance and series resistance were compensated electronically and values of cell input capacitance ( $C_i$ ) were noted. Current-voltage (IV) relations (measured from a holding voltage of -60 mV) were obtained by stepping the voltage to -100 mV and then ramping this value up to 0 mV over a period of 2.5 s. Membrane conductance was calculated from the slope of I-V relations between -90 and -50 mV (linear region). Changes in membrane voltage, firing frequency, and membrane conductance were quantified as the value observed during the last 30 s of the stimulus minus baseline (average of all points during 60 s before the stimulus).

### Single-Channel Recording

Recordings (d.c. -1 KHz) were obtained from isolated ONs using the cell-attached configuration of the patch-clamp technique with pipettes (3–6 M $\Omega$ ) filled with a solution comprising 140 mM NaCl, 3 mM KCl, 1 mM MgCl<sub>2</sub>, 10 mM HEPES, 10 mM tetraethylammonium chloride, 4 mM 4-aminopyridine, 1  $\mu$ M tetrodotoxin, and 0.1  $\mu$ M apamin (pH 7.4), osmolality 290 mosmol/kg. Pipette pressure was controlled using a high-speed pressure clamp ( $\tau$  = ~4 ms; HSPC-1; ALA Scientific Instruments) and monitored via a digital manometer (PMO15D; World Precision Instruments). Pressure-clamp experiments involved holding pipette pressure at 0 mmHg, and then delivering four consecutive 200 ms steps (separated by 1 s) during which pressure was increased to +2.5, +5, +10 and +20 mmHg. For each cell, we analyzed the effects of six consecutive pulses where no channel openings were observed during the 200 ms period preceding the pressure step, and where at least one opening was detected during the pulse. Only single-channel events >1 pA were analyzed.

### Immunohistochemistry on Tissue Sections

Rats were *trans*-cardiacally perfused with 10 ml of cytoskeletal buffer (CB) containing 130 mM NaCl, 10 mM MES, 5 mM EGTA, 5 mM MgCl<sub>2</sub>, 5 mM glucose, pH adjusted to 6.3; and then with 250 ml of CB containing 3% paraformaldehyde and 0.2% glutaraldehyde at 37°C. Brains were postfixed for at least 48 hr. Coronal sections (25  $\mu$ m thick) obtained using a vibratome were treated for 15 min in 0.1% NaBH<sub>4</sub> in CB. After a 1 hr incubation with 10% normal goat serum (in PBS containing 0.3% Triton-X), sections were washed and incubated overnight at 4°C with primary antibodies diluted in PBS. Following wash, sections were incubated for 1 hr with fluorescently labeled secondary antibodies (1:200) and DAPI (Life Technologies; 1:2000), mounted in SlowFade Gold Antifade reagent (Life Technologies), and observed using an FV1000 confocal microscope (Olympus Canada), or a structured illumination microscope using a Delta Vision OMX V<sub>4</sub> (Applied Precision).

### In Situ Proximity Ligation Assay

Sites at which tubulin and TRPV1 interact in situ were detected using the Duolink II fluorescence kit according to the manufacturer's instructions (Olink Bioscience) (Söderberg et al., 2006; Trifilieff et al., 2011). Briefly, acutely isolated neurons were fixed and permeabilized, then primary antibodies against  $\alpha$ -tubulin and TRPV1 were applied at 4°C overnight. Duolink secondary antibodies conjugated to oligonucleotides were then added and incubated at 37°C for 1 hr in a preheated humidity chamber. This was then followed by ligation and amplification using the kit's ligase and polymerase solution that also contained fluorescently labeled oligonucleotides. Signal is only generated if the two antigens are within 40 nm of each other. Control experiments used only one primary antibody or addition of TRPV1 antibody preadsorbed with a blocking (epitope) peptide (Alomone Labs). Samples were counterstained with DAPI and visualized using the confocal microscope.

### Immunohistochemistry and PLA on Isolated Neurons

Isolated cells were fixed for 15 min with CB containing 3% paraformaldehyde, 0.2% glutaraldehyde, and 0.25% Triton X-100 and washed with PBS at room temperature. Next, cells were treated for 15 min in 0.1% NaBH<sub>4</sub> in CB. After a 1 hr incubation with 2% normal goat serum (in PBS), cells were washed and incubated overnight at 4°C with primary antibodies. Following wash, cells were incubated for 1 hr with fluorescently labeled secondary antibodies (1:500) or processed for in situ PLA as described above.

### Analysis of Submembrane Microtubules

For membrane staining cell were fixed for 15 min with CB containing 3% paraformaldehyde, 0.2% glutaraldehyde, then incubated with 10  $\mu$ M CM-Dil (Life Technologies) for 30 min at 0°C, and postfixed with 3% paraformaldehyde for 30 min, washed with PBS, and slightly permeabilized with 0.2% of Triton X-100 for 90 s (Brandt et al., 1995). Next, cells were treated for 15 min in 0.1% NaBH<sub>4</sub> in CB. After a 1 hr incubation with 2% normal goat serum (in PBS), cells were washed and incubated overnight at 4°C with primary anti-tubulin antibodies. Following wash, cells were incubated for 1 hr with fluorescently-labeled secondary antibodies (1:500). Images were acquired using the structured illumination microscope. Because these cells were only treated very briefly with detergent (to minimize the loss of membrane structure), the pattern of Dil and microtubule staining varied over different parts of the cell due to regional differences in antibody penetration and membrane integrity. Thus for analysis, we only examined cell segments that showed a continuous stretch of Dil-labeled plasma membrane together with a high density of juxtaposed microtubules.

### Antibodies

$\alpha$ -tubulin mouse monoclonal antibody (DM1A, Sigma, 1:500), TRPV1 rabbit polyclonal antibody (and the inhibitory peptide to verify its specificity, Alomone labs, 1:200) directed against the C terminus of TRPV1, NeuN chicken polyclonal antibody (EMD Millipore; 1:500), vasopressin rabbit polyclonal antibody (VA4, 1:1000; provided by Dr. Hal Gainer, NIH) were used. Secondary antibodies were fluorescently-labeled Alexa-conjugated (488 nm, 568 nm, and 647 nm; Life Technologies).

### Structured Illumination Microscopy: 3D SIM

3D images of fixed samples were acquired using a structured microscope equipped with a 100 $\times$ /1.4 NA U-PLANAPO objective (Olympus Canada) and two Evolve EM-CCD cameras (Photometrics). Stacks of 48–80 optical sections (125 nm spacing) were acquired consecutively in three channels (405 nm, 488 nm, and 568 nm) using DeltaVision software (Applied Precision). Wide-field images were deconvolved using softWoRx image processing software (Applied Precision) using the enhanced ratio method. SIM images were reconstructed using softWoRx software using point spread function generated for each wavelength. The images presented and analyzed are maximal projections of z stack consisting of eight consecutive images representing fluorescence collected through 1  $\mu$ m of the tissue or cell (8  $\times$  125 nm). Brightness and contrast adjustments to images were subsequently made using ImageJ (NIH), and figures were compiled in CorelDRAW (Corel).

### Microtubule Complexity Analysis

A simplified assessment of microtubule network complexity was performed by examining the two-dimensional variance in the orientation of fibers detected in small areas of the cytoplasm. A small detection window was centered over a central region of the cytoplasm and lines of consistent length (3  $\mu$ m) were superimposed over all visible microtubules. The size of the window was expanded until a total of ten microtubules had been skeletonized and then the angles of each line were determined. Variance was computed as the square of the standard deviation of the angles measured in each case.

### Synthetic TRPV1 Peptides

Three 21 amino acid peptides whose sequences corresponded to portions of the C terminus of rat TRPV1 (Figure S3; synthesized by American Peptide) were dissolved as 70 mM stocks in DMSO and diluted to a final concentration of 70  $\mu$ M in the patch pipette. The amino acid sequences of peptide 1 (P1) corresponded to the  $\beta$ -tubulin domain 1; peptide 2 (P2) corresponded to the  $\beta$ -tubulin domain 2; and peptide 3 (P3) corresponded to the most distal part of the C terminus of TRPV1 and served as a control for P1 and P2. The amino acid sequences are listed from N terminus to C terminus: P1: Lys - Ser - Phe - Leu - Lys - Cys - Met - Arg - Lys - Ala - Phe - Arg - Ser - Gly - Lys - Leu - Leu - Gln - Val - Gly - Phe; P2: Lys - Arg - Thr - Leu - Ser - Phe -Ser - Leu - Arg - Ser - Gly - Arg - Val - Ser - Gly - Arg - Asn - Trp - Lys - Asn - Phe; P3: Thr - Gly - Ser - Leu - Lys - Pro - Glu - Asp - Ala - Glu - Val - Phe - Lys - Asp - Ser - Met - Val - Pro - Gly - Glu - Lys. The amino acid sequences of P1 and P2

have less than 53% homology to other TRPV proteins (Goswami and Hucho, 2008).

#### Coimmunoprecipitation

For immunoprecipitation (IP), tissue blocks containing the SON were removed from 8 adult rats and homogenized in ice-cold IP buffer containing 20 mM Tris-HCl (pH 7.4), 150 mM NaCl, 1 mM EDTA, 1% (w/v) dodecyl maltoside, 5 mM NaF; 1.5 mM Na<sub>3</sub>VO<sub>4</sub> and protease inhibitor cocktail (complete, EDTA-free; Roche Diagnostics, Laval QC). Following centrifugation at 3,000 × g for 10 min, the supernatant was precleared on protein G agarose beads (Millipore) at 4°C for 1 hr. The precleared cell lysate was incubated at 4°C overnight with beads covalently crosslinked to TRPV1 antibodies. In some experiments the P1, P2, and P3 peptides were added to the reaction (5 μg per 10 μg of the crosslinked antibody). Then the beads were washed four times with IP buffer and proteins were eluted with sample buffer followed by SDS-PAGE and western blotting. Briefly, following electrophoresis, proteins were transferred to 0.2 μm nitrocellulose membranes. Membranes were blocked in 5% dry milk powder in Tris-buffered saline containing 0.1% Tween-20 for 1 hr prior to overnight incubation with α-tubulin antibody. The membranes were then washed, incubated for 1 hr with HRP-conjugated secondary antibody, washed again, treated with Enhanced Chemiluminescence reagent (Perkin Elmer), and exposed to autoradiography films (Denville Scientific). All signals were obtained in the linear range for each antibody and quantified using ImageJ (NIH). To crosslink protein G agarose beads to antibody, the beads were first washed in 0.2 M triethanolamine (pH 9.0) and then incubated with the antibody (10 μg of antibody per 30 μl of packed beads) for 1 hr at room temperature in the presence of dimethyl pimelimidate dihydrochloride (15 mg/ml). After 1 hr, the beads were washed with 0.2 M triethanolamine (pH 9.0) for 60 min at RT with rotation and then resuspended in the IP buffer. Inhibitory peptide (1 μg per 1 μg of TRPV1 antibody) was incubated for 1 hr at room temperature with crosslinked beads before IP.

#### Statistical Analysis

All results are expressed as mean ± SEM. All statistical comparisons were made with either Student's t test or a one-way ANOVA followed by between-group comparisons using Tukey's post hoc test, with p < 0.05 as significance criteria. \*p < 0.05, \*\*p < 0.01, and \*\*\*p < 0.001.

#### SUPPLEMENTAL INFORMATION

Supplemental Information includes six figures and can be found with this article online at <http://dx.doi.org/10.1016/j.neuron.2014.07.023>.

#### AUTHOR CONTRIBUTIONS

M.P.K. and C.W.B. designed the experiments; M.P.K. and A.K. performed the experiments, and M.P.K. and C.W.B. wrote the paper.

#### ACKNOWLEDGMENTS

This work was supported by operating grants FRN82818 and MOP9939 from the Canadian Institutes of Health Research to C.W.B. and by a James McGill Chair awarded to C.W.B. by McGill University. M.P.K. was supported in part by a Postdoctoral Fellowship Award from the Heart and Stroke Foundation of Canada. The Research Institute of the McGill University Health Center receives generous support from Le Fonds de recherche du Québec – Santé. The authors thank Drs. B. Geiger, R. Sharif-Naeini, S.H. Oliet, U. Ashery, and W. Liedtke for constructive comments on an early draft of this manuscript. We also thank Dr. Hal Gainer (NIH, Bethesda, MD) for supplying some of the antibodies used in our experiments, and Drs. E. Küster-Schöck and J. Lacoste (McGill CIAN Microscopy Facility) for technical support with structured illumination microscopy.

Accepted: July 10, 2014

Published: August 7, 2014

#### REFERENCES

- Baas, P.W., and Ahmad, F.J. (2013). Beyond taxol: microtubule-based treatment of disease and injury of the nervous system. *Brain* 136, 2937–2951.
- Baas, P.W., Sinclair, G.I., and Heidemann, S.R. (1987). Role of microtubules in the cytoplasmic compartmentation of neurons. *Brain Res.* 420, 73–81.
- Bourque, C.W. (1989). Ionic basis for the intrinsic activation of rat supraoptic neurones by hyperosmotic stimuli. *J. Physiol.* 417, 263–277.
- Bourque, C.W. (2008). Central mechanisms of osmosensation and systemic osmoregulation. *Nat. Rev. Neurosci.* 9, 519–531.
- Brandt, R., Léger, J., and Lee, G. (1995). Interaction of tau with the neural plasma membrane mediated by tau's amino-terminal projection domain. *J. Cell Biol.* 131, 1327–1340.
- Brangwynne, C.P., MacKintosh, F.C., Kumar, S., Geisse, N.A., Talbot, J., Mahadevan, L., Parker, K.K., Ingber, D.E., and Weitz, D.A. (2006). Microtubules can bear enhanced compressive loads in living cells because of lateral reinforcement. *J. Cell Biol.* 173, 733–741.
- Burton, P.R. (1992). Ultrastructural studies of microtubules and microtubule organizing centers of the vertebrate olfactory neuron. *Microsc. Res. Tech.* 23, 142–156.
- Cao, E., Liao, M., Cheng, Y., and Julius, D. (2013). TRPV1 structures in distinct conformations reveal activation mechanisms. *Nature* 504, 113–118.
- Chakfe, Y., and Bourque, C.W. (2000). Excitatory peptides and osmotic pressure modulate mechanosensitive cation channels in concert. *Nat. Neurosci.* 3, 572–579.
- Chalfie, M. (2009). Neurosensory mechanotransduction. *Nat. Rev. Mol. Cell Biol.* 10, 44–52.
- Chalfie, M., and Au, M. (1989). Genetic control of differentiation of the *Caenorhabditis elegans* touch receptor neurons. *Science* 243, 1027–1033.
- Chalfie, M., and Sulston, J. (1981). Developmental genetics of the mechanosensory neurons of *Caenorhabditis elegans*. *Dev. Biol.* 82, 358–370.
- Cheng, L.E., Song, W., Looger, L.L., Jan, L.Y., and Jan, Y.N. (2010). The role of the TRP channel NompC in *Drosophila* larval and adult locomotion. *Neuron* 67, 373–380.
- Christensen, A.P., and Corey, D.P. (2007). TRP channels in mechanosensation: direct or indirect activation? *Nat. Rev. Neurosci.* 8, 510–521.
- Ciura, S., and Bourque, C.W. (2006). Transient receptor potential vanilloid 1 is required for intrinsic osmoreception in organum vasculosum lamina terminalis neurons and for normal thirst responses to systemic hyperosmolality. *J. Neurosci.* 26, 9069–9075.
- Ciura, S., Liedtke, W., and Bourque, C.W. (2011). Hypertonicity sensing in organum vasculosum lamina terminalis neurons: a mechanical process involving TRPV1 but not TRPV4. *J. Neurosci.* 31, 14669–14676.
- Dogterom, M., Kerssemakers, J.W., Romet-Lemonne, G., and Janson, M.E. (2005). Force generation by dynamic microtubules. *Curr. Opin. Cell Biol.* 17, 67–74.
- Downing, K.H. (2000). Structural basis for the interaction of tubulin with proteins and drugs that affect microtubule dynamics. *Annu. Rev. Cell Dev. Biol.* 16, 89–111.
- Fletcher, D.A., and Mullins, R.D. (2010). Cell mechanics and the cytoskeleton. *Nature* 463, 485–492.
- Goswami, C., and Hucho, T. (2008). Submembrane microtubule cytoskeleton: biochemical and functional interplay of TRP channels with the cytoskeleton. *FEBS J.* 275, 4684–4699.
- Goswami, C., Dreger, M., Jahnel, R., Bogen, O., Gillen, C., and Hucho, F. (2004). Identification and characterization of a Ca<sup>2+</sup>-sensitive interaction of the vanilloid receptor TRPV1 with tubulin. *J. Neurochem.* 91, 1092–1103.
- Goswami, C., Hucho, T.B., and Hucho, F. (2007). Identification and characterization of novel tubulin-binding motifs located within the C-terminus of TRPV1. *J. Neurochem.* 101, 250–262.
- Hoffman, B.D., Grashoff, C., and Schwartz, M.A. (2011). Dynamic molecular processes mediate cellular mechanotransduction. *Nature* 475, 316–323.

- Ingber, D.E. (2003). Tensegrity I. Cell structure and hierarchical systems biology. *J. Cell Sci.* *116*, 1157–1173.
- Janson, M.E., de Dood, M.E., and Dogterom, M. (2003). Dynamic instability of microtubules is regulated by force. *J. Cell Biol.* *161*, 1029–1034.
- Jaworski, J., Kapitein, L.C., Gouveia, S.M., Dortland, B.R., Wulf, P.S., Grigoriev, I., Camera, P., Spangler, S.A., Di Stefano, P., Demmers, J., et al. (2009). Dynamic microtubules regulate dendritic spine morphology and synaptic plasticity. *Neuron* *61*, 85–100.
- Jordan, M.A., Thrower, D., and Wilson, L. (1992). Effects of vinblastine, podophyllotoxin and nocodazole on mitotic spindles. Implications for the role of microtubule dynamics in mitosis. *J. Cell Sci.* *102*, 401–416.
- Liang, X., Madrid, J., Gärtner, R., Verbavatz, J.M., Schiklenk, C., Wilsch-Bräuninger, M., Bogdanova, A., Stenger, F., Voigt, A., and Howard, J. (2013). A NOMPC-dependent membrane-microtubule connector is a candidate for the gating spring in fly mechanoreceptors. *Curr. Biol.* *23*, 755–763.
- Luxton, G.W., and Gundersen, G.G. (2011). Orientation and function of the nuclear-centrosomal axis during cell migration. *Curr. Opin. Cell Biol.* *23*, 579–588.
- Marshall, K.L., and Lumpkin, E.A. (2012). The molecular basis of mechanosensory transduction. *Adv. Exp. Med. Biol.* *739*, 142–155.
- Mason, W.T. (1980). Supraoptic neurones of rat hypothalamus are osmosensitive. *Nature* *287*, 154–157.
- Nixon, R.A. (1998). Dynamic behavior and organization of cytoskeletal proteins in neurons: reconciling old and new findings. *Bioessays* *20*, 798–807.
- O'Hagan, R., Chalfie, M., and Goodman, M.B. (2005). The MEC-4 DEG/ENaC channel of *Caenorhabditis elegans* touch receptor neurons transduces mechanical signals. *Nat. Neurosci.* *8*, 43–50.
- Oliet, S.H., and Bourque, C.W. (1992). Properties of supraoptic magnocellular neurones isolated from the adult rat. *J. Physiol.* *455*, 291–306.
- Oliet, S.H., and Bourque, C.W. (1993a). Mechanosensitive channels transduce osmosensitivity in supraoptic neurons. *Nature* *364*, 341–343.
- Oliet, S.H., and Bourque, C.W. (1993b). Steady-state osmotic modulation of cationic conductance in neurons of rat supraoptic nucleus. *Am. J. Physiol.* *265*, R1475–R1479.
- Samson, F., Donoso, J.A., Heller-Bettinger, I., Watson, D., and Himes, R.H. (1979). Nocodazole action on tubulin assembly, axonal ultrastructure and fast axoplasmic transport. *J. Pharmacol. Exp. Ther.* *208*, 411–417.
- Sharif-Naeini, R., Witty, M.F., Séguéla, P., and Bourque, C.W. (2006). An N-terminal variant of Trpv1 channel is required for osmosensory transduction. *Nat. Neurosci.* *9*, 93–98.
- Sharif-Naeini, R., Folgering, J.H., Bichet, D., Duprat, F., Lauritzen, I., Arhatte, M., Jodar, M., Dedman, A., Chatelain, F.C., Schulte, U., et al. (2009). Polycystin-1 and -2 dosage regulates pressure sensing. *Cell* *139*, 587–596.
- Söderberg, O., Gullberg, M., Jarvius, M., Ridderstråle, K., Leuchowius, K.J., Jarvius, J., Wester, K., Hydbring, P., Bahram, F., Larsson, L.G., and Landegren, U. (2006). Direct observation of individual endogenous protein complexes in situ by proximity ligation. *Nat. Methods* *3*, 995–1000.
- Stepanova, T., Slemmer, J., Hoogenraad, C.C., Lansbergen, G., Dortland, B., De Zeeuw, C.I., Grosveld, F., van Cappellen, G., Akhmanova, A., and Galjart, N. (2003). Visualization of microtubule growth in cultured neurons via the use of EB3-GFP (end-binding protein 3-green fluorescent protein). *J. Neurosci.* *23*, 2655–2664.
- Stiess, M., and Bradke, F. (2011). Neuronal polarization: the cytoskeleton leads the way. *Dev. Neurobiol.* *71*, 430–444.
- Storti, B., Bizzarri, R., Cardarelli, F., and Beltram, F. (2012). Intact microtubules preserve transient receptor potential vanilloid 1 (TRPV1) functionality through receptor binding. *J. Biol. Chem.* *287*, 7803–7811.
- Topalidou, I., Keller, C., Kalebic, N., Nguyen, K.C., Somhegyi, H., Politi, K.A., Heppenstall, P., Hall, D.H., and Chalfie, M. (2012). Genetically separable functions of the MEC-17 tubulin acetyltransferase affect microtubule organization. *Curr. Biol.* *22*, 1057–1065.
- Trifilieff, P., Rives, M.L., Urizar, E., Piskorowski, R.A., Vishwasrao, H.D., Castrillon, J., Schmauss, C., Slättman, M., Gullberg, M., and Javitch, J.A. (2011). Detection of antigen interactions ex vivo by proximity ligation assay: endogenous dopamine D2-adenosine A2A receptor complexes in the striatum. *Biotechniques* *51*, 111–118.
- Tyler, W.J. (2012). The mechanobiology of brain function. *Nat. Rev. Neurosci.* *13*, 867–878.
- Vignaud, T., Blanchoin, L., and Théry, M. (2012). Directed cytoskeleton self-organization. *Trends Cell Biol.* *22*, 671–682.
- Yan, Z., Zhang, W., He, Y., Górczyca, D., Xiang, Y., Cheng, L.E., Meltzer, S., Jan, L.Y., and Jan, Y.N. (2013). *Drosophila* NOMPC is a mechanotransduction channel subunit for gentle-touch sensation. *Nature* *493*, 221–225.
- Zhang, Z., and Bourque, C.W. (2003). Osmometry in osmosensory neurons. *Nat. Neurosci.* *6*, 1021–1022.
- Zhang, Z., Kindrat, A.N., Sharif-Naeini, R., and Bourque, C.W. (2007). Actin filaments mediate mechanical gating during osmosensory transduction in rat supraoptic nucleus neurons. *J. Neurosci.* *27*, 4008–4013.